Record-low thermospheric density during the 2008 solar minimum

J. T. Emmert[1], J. L. Lean[1], J. M. Picone[2]

[1]Space Science Division, Naval Research Laboratory
[2]Department of Physics and Astronomy, George Mason University

We use global-average thermospheric total mass density, derived from the drag effect on the orbits of many space objects, to study the behavior of the thermosphere during the prolonged minimum in solar activity between cycles 23 and 24. During 2007–2009 thermospheric densities at a fiducial altitude of 400 km were the lowest observed in the 43-year database, and were anomalously low, by 10–30%, compared with climatologically expected levels. The density anomalies appear to have commenced before 2006, well before the cycle 23/24 minimum, and are larger than expected from enhanced thermospheric cooling by increasing concentrations of CO_2. The height dependence of the mass density anomalies suggests that they are attributable to a combination of lower-than-expected exospheric temperature (–14 K) and reductions in the number density of atomic oxygen (–12%) and other species (–3%) near the base of the diffusive portion of the thermosphere.

1. Introduction

In Earth's thermosphere, density at a fixed geometric height is highly sensitive to variations of solar irradiance at extreme ultraviolet (EUV) wavelengths (0–120 nm). EUV and far ultraviolet (FUV) photons are the primary heat source of the thermosphere [*Roble*, 1995], which expands and contracts in response to temperature changes. Solar EUV irradiance increases by a factor of 2 or more from the minimum to maximum of the 11-year solar activity cycle [*Lean*, 1997], driving order-of-magnitude increases of total mass density near 400 km [e.g., *Emmert and Picone*, 2010]. Cycle 23 (1996.4–2008.8, 12.4 years long) was unusually prolonged relative to prior cycles 22 (9.7 years) and 21 (10.3 years). The minimum of cycle 23/24 had the most days without sunspots since the 1933 minimum [*Livingston and Penn*, 2009]. In response to corresponding prolonged low levels of solar EUV irradiance during this period, the thermosphere is expected to have been unusually cool and contracted. Measurements of ion temperatures [*Heelis et al.*, 2009] provide indirect evidence of this.

Steady increases in atmospheric CO_2 concentrations complicate the interpretation of thermospheric behavior during the cycle 23/24 minimum because CO_2 in the lower thermosphere is the thermosphere's dominant cooling agent [*Roble*, 1995]. Increased concentrations of CO_2 and other greenhouse gases (such as CH_4) are expected to produce a cooler, more contracted thermosphere [*Roble and Dickinson*, 1989]. Empirical support for this expected thermospheric climate change has been reported [e.g., *Emmert et al.*, 2008], including enhanced density depletion during solar minimum epochs.

The historical archive of orbital data for the thousands of man-made objects that orbit Earth provides unique, continuous, and self-consistent information on the state of the thermosphere over many decades. In this paper, we employ these data to compare the behavior of the thermosphere during the current solar minimum with that of the previous three solar minima.

2. Data

We use the 40-year database of globally averaged mass density described by *Emmert* [2009], which we have extended through January 2010 without incorporating new objects. The data, derived from the orbits of thousands of objects, cover the period 1967–2010 and consist of daily values as a function of altitude between 200 and 600 km with temporal resolution of 3–6 days.

We also employ four decades of continuously measured 10.7 cm solar radio flux ($F_{10.7}$) as a proxy for EUV irradiance. Although the statistical relationship between daily EUV and $F_{10.7}$ is somewhat nonlinear [*Liu et al.*, 2006], $F_{10.7}$ has proven empirically to be a reliable, well calibrated indicator of thermospheric density variations (including during solar minima), and its 81-day mean values closely track indices of solar chromospheric activity. Crucial for our application, $F_{10.7}$ is the only extant record of solar irradiance covering the past four solar activity cycles. Continuous measurements of solar EUV irradiance with adequate stability commence only in 2002 with the launch of the TIMED/SEE instrument, and EUV proxies based on solar spectral features (such as the Mg or Ca K indices) are available only after 1976 [*Lean et al.*, 2001]. Long-term calibration of these measurements and proxies is challenging, and they lack the temporal stability of the continuous, well calibrated [*Tapping*, 1994] $F_{10.7}$ index.

We remove seasonal and geomagnetic activity effects from the density data by subtracting the variations predicted by a modified version of the empirical Global Average Mass Density Model (GAMDM) [*Emmert and Picone*, 2010]. GAMDM is based on the 1986–2007 portion of the density database and represents global-average density at a given altitude as a function of the daily and 81-day average $F_{10.7}$, the day of year, and the daily *Kp* geomagnetic activity index. The modified version employed here uses $F_{10.7}$ normalized

to 1 AU (rather than at the Earth-sun distance) which causes density variations associated with Earth's orbital eccentricity to be incorporated in the day-of-year terms, rather than the solar terms [*Emmert and Picone*, 2010]. The filtered densities are thus largely free of Earth-orbit effects, annual-scale harmonics, and geomagnetic activity influences.

3. Results

3.1. Summary of the historical record

Figure 1a shows the filtered daily global-average density data at 400 km from 1967 through January 2010. The density in 2008 was unequivocally lower than at any time in this historical record, as indicated by the horizontal dotted line. It was also the lowest since the beginning of the space age in 1957, when the derivation of thermospheric density from orbital motion became possible.

In contrast to the density time series, solar minimum $F_{10.7}$ irradiances (Figure 1b) have remained approximately constant over the last four minima. Figures 1c and 1d show 81-day running averages of log-density and $F_{10.7}$ ($\bar{F}_{10.7}$), respectively. On this time scale, the minimum density during cycle 23/24 was 28% lower than that during cycle 22/23 (after filtering seasonal and geomagnetic activity effects). This decrease is considerably larger than the 6% change expected from the long-term downward linear trend [*Emmert et al.*, 2008] over the previous three solar minima. $\bar{F}_{10.7}$ also exhibits a decrease, of 3.7%, between the cycle 22/23 and 23/24 minima. In addition to the known statistical dependence of thermospheric density on $\bar{F}_{10.7}$, there is some indication that the thermosphere responds to EUV variations on time scales up to 81 days [*Emmert and Picone*, 2010, section 5.1]. Therefore, the decrease in $\bar{F}_{10.7}$ may explain some of the density difference.

3.2. Comparison of last four solar minima

To characterize the development of the unusually low thermospheric densities, Figure 2 superposes the last four solar minima. Figure 2a shows $\bar{F}_{10.7}$ shifted to align the times of the minima in the running annual average $F_{10.7}$. Figure 2b shows corresponding density anomalies relative to the full GAMDM: that is, departures from the 1986–2007, $F_{10.7}$-dependent climatology. The absence of large systematic deviations among the first three minima demonstrates the long-term consistency of $\bar{F}_{10.7}$ as an indicator of thermospheric density, at least from 1967 to 2005. Large negative anomalies began to appear at the end of 2005, and by 2007 the densities were well outside the inter-cycle variability among the previous three minima.

Figure 3a shows the cycle 23/24 minimum in more detail. A qualitatively strong correspondence between the density variations and $\bar{F}_{10.7}$ is evident throughout this time period. Although there is some indication that $F_{10.7}$ is a less sensitive indicator of EUV emission variations during solar minimum than at other phases of the solar cycle [*Viereck et al.*, 2001], Figure 3a suggests that it retains an association with EUV at solar minimum.

Figure 3b depicts the evolution of the cycle 23/24 density as a function of $\bar{F}_{10.7}$. At epoch 1, just before 2006, the density levels were below the GAMDM climatology (solid black line). The offset became larger by epoch 2, but from epoch 2 to epoch 3 the trajectory largely paralleled the climatology. Between epochs 2 and 3, around 2007.6, $\bar{F}_{10.7}$ values decreased below those of the previous minima, so that the GAMDM predictions are an extrapolation of the climatology. Between epochs 3 and 4, density increased along with $\bar{F}_{10.7}$, but not as steeply as GAMDM, and the magnitude of the anomaly therefore increased. After epoch 4, a prolonged period of very little daily variation in $F_{10.7}$ began. Density decreased to its overall minimum at epoch 5, and $\bar{F}_{10.7}$ reached its minimum at epoch 6. Coming out of the minimum, density exhibited the largest departures (about 30%) from climatology at epoch 7, and then recovered to within 15% of the climatology by epoch 8 (2010.0). Overall, Figure 3b suggests that density generally paralleled the climatology during individual periods of $\bar{F}_{10.7}$ increases and decreases, but gradually drifted away from the climatology until about 2009.5.

3.3. Vertical structure and interpretation

Figures 2 and 3 demonstrate that density at 400 km was anomalously low during the cycle 23/24 solar minimum. To understand how the state of the thermosphere differed from that represented by the $F_{10.7}$-dependent GAMDM climatology, we investigated the height dependence of the average relative density anomalies during the year centered on 2008.8 (the actual solar minimum epoch), as shown in Figure 4. On the temporal and spatial scales of the orbit-derived density data (3–6 days), the thermosphere may be assumed to be in diffusive equilibrium above ~150 km [*Meier et al.*, 2001]. At solar minimum, O is the dominant species between about 180 and 520 km.

To decompose the mass density anomaly profile in terms of temperature and composition changes, we perturbed the parameters of a baseline Bates-Walker (BW) diffusive equilibrium profile [*Bates*, 1959; *Walker*, 1965; *Hedin*, 1987] until the resulting mass density relative changes optimally (least-squares) matched the observed anomalies. Our forward model is thus $\left(\rho^{BW}-\rho_0^{BW}\right)/\rho_0^{BW}$ and our target data are $\left(\rho-\rho^{M}\right)/\rho^{M}$, where ρ^{BW} and ρ_0^{BW} are respectively the perturbed and baseline BW density profiles, ρ is the observed density, and ρ^M is the GAMDM density. The BW profile $n_i(z)$, $T(z)$ (where n_i is the number density of species i and T is the temperature) is specified by T_{ex}, the asymptotic thermospheric temperature; T_l and T_l', the temperature and its gradient at the lower boundary height z_l; and by $n_i(z_l)$, the number density of species i at z_l.

For the baseline BW profile, we used parameters from the NRLMSISE-00 [*Picone et al.*, 2002] empirical thermosphere model, which employs the BW diffusive profile. The NRLMSISE-00 parameters for the conditions represented by the data in Figure 4 are: T_{ex} = 727 K, T_l = 356 K, T_l' = 12.4 K/km, and composition (by number density) at z_l = 120 km

that includes 79.0% N_2, 17.2% O, 3.40% O_2, and 0.00623% He.

An optimal density perturbation profile obtained by varying only T_{ex} (dotted line, Figure 4) does not match the observations well, indicating that exospheric temperature changes alone cannot explain the density anomalies. Allowing the number density at the lower boundary (z_l = 120 km) also to vary (without changing composition) provides a better fit (dashed line, Figure 4), but the shape still differs somewhat from the observations. Only when the density of O at 120 km is allowed to vary independently of the other species does the fit (solid line) match the observed perturbation profile. These results are consistent with attribution of the anomalously low mass densities during the cycle 23/24 minimum to a combination of low exospheric temperatures (–14 K) and lower-boundary number densities (–12% for O and –3% for other species).

The inferred temperature and composition perturbations are only weakly dependent on the baseline conditions, so any errors in the NRLSMSISE-00 baseline specifications should not significantly affect the results. The mass density perturbation profile peaks near 500 km because this is the transition region from O to He; n_{He} decreases less rapidly with height than n_O. As noted by *Emmert* [2009], the orbit-derived density data may contain some altitude-dependent bias due to dependences, not fully accounted for in the derivation, of satellite drag coefficients on composition (and hence altitude). However, the perturbation densities shown in Figure 4 should be largely free of such bias because it affects both the data and the reference climatology at solar minimum.

4. Discussion

After filtering out seasonal and geomagnetic activity effects, the average density at 400 km during the year surrounding the cycle 23/24 minimum was 29% lower than the corresponding average density during the cycle 22/23 minimum (almost the same as the 28% difference, shown in Figure 1c, between the minimum 81-day average densities in 1996 and 2008). About 10% (i.e., one-third) of this 29% difference is attributable to lower $\bar{F}_{10.7}$ values during the cycle 23/24 minimum. The remaining 19% (two-thirds) of the 29% difference is anomalous; i.e., not attributable to the GAMDM-estimated climatological effect of prolonged low levels of solar EUV irradiance (for which $F_{10.7}$ is a proxy) or geomagnetic activity during the cycle 23/24 minimum. Model simulations [*Qian et al.*, 2006] suggest that a 3% decrease is explainable by greater CO_2 cooling than during the cycle 22/23 minimum 12 years earlier, and observed linear density trends over the previous three solar minima [*Emmert et al.*, 2008] suggest that densities should be 6% lower than the previous minimum. So 13–16% (i.e., about half) of the observed inter-minima difference remains unexplained by theoretical and experimental work to date.

Accounting for the anomalously low thermospheric density solely in terms of reduced solar EUV irradiance requires that the long-term relationship between EUV irradiance and $F_{10.7}$ has changed markedly during recent years (beginning around 2006) compared to the previous three decades, with EUV levels decreasing more than expected from the $F_{10.7}$ proxy, resulting in less thermospheric heating. As the only major departure of $F_{10.7}$ as a suitable EUV indicator since 1967, this explanation represents a solar (rather than terrestrial) anomaly.

The composition changes illustrated in Figure 4, which can account for about half the anomalous density decrease, may accrue from changes in the chemical and dynamical processes of the underlying mesosphere and lower thermosphere (MLT) that affect the concentration of O at the base of the thermosphere. Internal MLT processes possibly in combination with longer-term anthropogenic changes are therefore appealing candidates for explaining the density changes. In addition to enhanced radiative cooling by CO_2 and CH_4, changes in two other MLT minor species, O_3 and H_2O, also influence thermospheric densities [*Akmaev et al.*, 2006], but trends in these latter species were small during cycle 23 [*Randel and Wu*, 2007; *Nedoluha et al.*, 2009].

Prior work has established that greenhouse-gas cooling of the thermosphere is enhanced during solar minima, a relationship that the prolonged (by more than a year) 2008 minimum may have amplified. If changes in the radiative properties of the MLT are responsible for the temperature and composition changes of the upper thermosphere, then the density anomalies may signify that an as yet unidentified climatological tipping point, involving energy balance and chemistry feedbacks, has been reached.

Further research is needed to clarify the sources of the observed density anomalies. Direct evidence for a shift in the $F_{10.7}$-EUV relationship would require reliable independent estimates of the latter and additional density analysis using EUV measurements and other proxies. A more detailed, time-dependent deconstruction of the density anomalies such as that of section 3.3 would elucidate how the anomalies developed, and analysis of other thermospheric, ionospheric, and mesospheric data (e.g., TIMED/GUVI, total electron content, and TIMED/SABER) would provide a fuller picture. Finally, the manner in which the thermosphere continues to recover from the cycle 23/24 minimum and its behavior during the next minimum should provide more clues as to the sources of the anomalies.

Acknowledgements

This work was supported by the Office of Naval Research and NASA's Causes and Consequences of the Minimum of Solar Cycle 24 Program (Grant NNH10AN62I).

References

Akmaev, R. A., V. I. Fomichev, and X. Zhu (2006), Impact of middle-atmospheric composition changes on greenhouse cooling in the upper atmosphere, *J. Atmos. Solar-Terr. Phys.*, *68*, 1879–1889.

Bates, D. R. (1959), Some problems concerning the terrestrial atmosphere above about the 100 km level, *Proc. R. Soc. London, Ser. A*, *253*, 451–462.

Emmert, J. T. (2009), A long-term data set of globally averaged thermospheric total mass density, *J. Geophys Res.*, *114*, A06315, doi:10.1029/2009JA014102.

Emmert, J. T., and J. M. Picone (2010), Climatology of globally averaged thermospheric mass density, *J. Geophy. Res.*, Paper 2010JA015298, in press.

Emmert, J. T., J. M. Picone, and R. R. Meier (2008), Thermospheric global average density trends, 1967–2007,

derived from orbits of 5000 near-Earth objects, *Geophys. Res. Lett.*, *35*, L05101, doi:10.1029/2007GL032809.
Hedin, A. E. (1987), MSIS-86 thermospheric model, *J. Geophys Res.*, *92*, 4649–4662.
Heelis, R. A., W. R. Coley, A. G. Burrell, M. R. Hairston, G. D. Earle, M. D. Perdue, R. A. Power, L. L. Harmon, B. J. Holt, and C. R. Lippincott (2009), Behavior of the O+/H+ transition height during the extreme solar minimum of 2008, *Geophys. Res. Lett.*, *36*, L00C03, doi:10.1029/2009GL038652.
Lean, J. L. (1997), The Sun's variable radiation and its relevance for Earth, *Annu. Rev. Astron. Astrophys.*, *35*, 33–67.
Lean, J. L., O. R. White, W. C. Livingston, and J. M. Picone (2001), Variability of a composite chomospheric irradiance index during the 11-year activity cycle and over longer time periods, *J. Geophys Res.*, *106*, 10,645–10,658.
Liu, L., W. Wan, B. Ning, O. M. Pirog (2006), Solar activity variations of the ionospheric peak electron density, *J. Geophys Res.*, *111*, A08304, doi:10.1029/2006JA011598.
Livingston, W., and M. Penn (2009), Are Sunspots Different During This Solar Minimum?, *Eos Trans. AGU*, *90*(30), p. 257–258.
Meier, R. R., J. M. Picone, D. P. Drob, and R. G. Roble (2001), Similarity transformation-based analysis of atmospheric models, data, and inverse remote sensing algorithms, *J. Geophys Res.*, *106*, 15,519–15,532.
Nedoluha, G. E., R. M. Gomez, B. C. Hicks, J. E. Wrotny, C. Boone, and A. Lambert (2009), Water vapor measurements in the mesosphere from Mauna Loa over solar cycle 23, *J. Geophys Res.*, *114*, D23303, doi:10.1029/2009JD012504.
Picone, J. M., A. E. Hedin, D. P. Drob, and A. C. Aikin (2002), NRLMSISE-00 empirical model of the atmosphere: Statistical comparisons and scientific issues, *J. Geophys Res.*, *107*, doi:10.1029/2002JA009430.
Qian, L., R. G. Roble, S. C. Solomon, and T. J. Kane (2006), Calculated and observed climate change in the thermosphere, and a prediction for solar cycle 24, *Geophys. Res. Lett.*, *33*, L23705, doi:10.1029/2006GL027185.
Randel, W. J., and F. Wu (2007), A stratospheric ozone profile data set for 1979–2005: Variability, trends, and comparisons with column ozone data, *J. Geophys Res.*, *112*, D06313, doi:10.1029/2006JD007339.
Roble, R. G. (1995), Energetics of the mesosphere and thermosphere, The Upper Mesosphere and Lower Thermosphere, *Geophys. Monogr. Ser.*, *87*, 1–21.
Roble, R. G., and R. E. Dickinson (1989), How will changes in carbon dioxide and methane modify the mean structure of the mesosphere and thermosphere?, *Geophys. Res. Lett.*, *16*, 1441–1444.
Tapping, K. F., and D. P. Charrois (1994), Limits to the accuracy of the 10.7 cm flux, *Solar Phys.*, *150*, 305–315.
Viereck, R., L. Puga, D. McMullin, D. Judge, M. Weber, and W. K. Tobiska (2001), The Mg II Index: A Proxy for Solar EUV, *Geophys. Res. Lett.*, *28*, 1343–1346.
Walker, J. C. G. (1965), Analytic Representation of Upper Atmosphere Densities Based on Jacchia's Static Diffusion Models, *J. Atmos. Sci.*, *22*, 462–463.

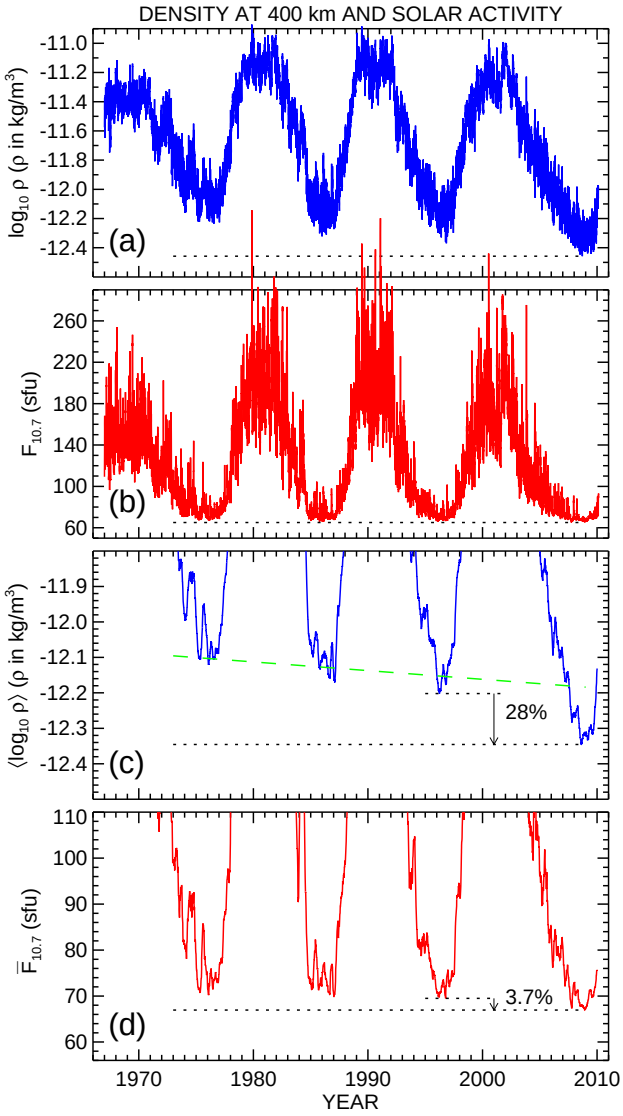

Figure 1. (a) Daily global-average mass log-density (seasonal and geomagnetic activity effects removed) at a fiducial altitude of 400 km. The dotted horizontal line indicates the minimum overall density. (b) The daily 10.7 cm solar radio flux ($F_{10.7}$) normalized to 1 AU, in solar flux units (sfu, 10^{-22} W m^{-2} Hz^{-1}). (c) Same as (a), but showing the running 81-day average log-densities. The green dashed line shows the solar minimum density trend reported by *Emmert et al.* [2008]. (d) Same as (b), but showing the 81-day average $F_{10.7}$ ($\bar{F}_{10.7}$). The horizontal dotted lines in (c) and (d) illustrate the differences between the cycle 23/24 and cycle 22/23 minima.

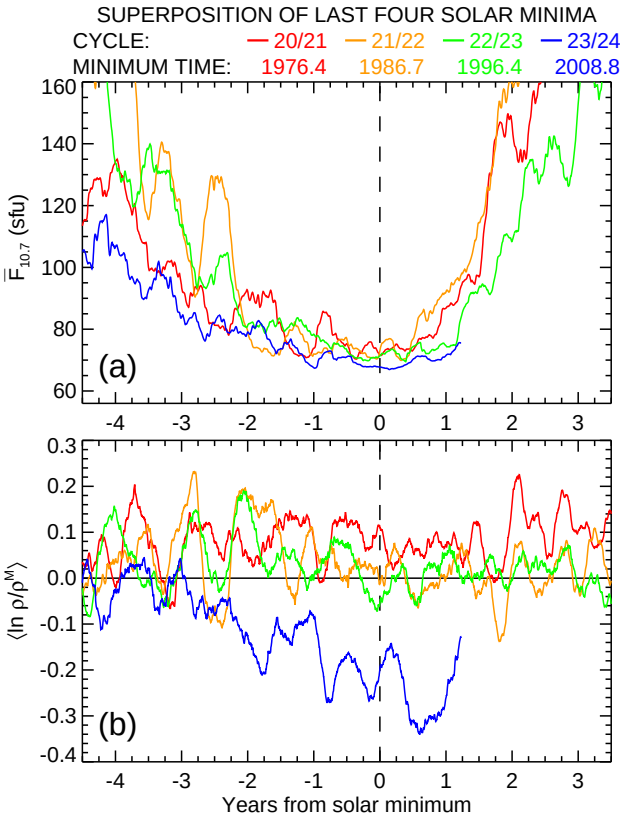

Figure 2. (a) Superposition of $\bar{F}_{10.7}$ during the last four solar minima. The black vertical dashed line indicates the time of the minimum of the running annual average $F_{10.7}$ for cycle 20/21 (red line), cycle 21/22 (orange), cycle 22/23 (green), and cycle 23/24 (blue). The solar minimum epochs are indicated above the plot. (b) Superposition of density anomalies (relative to the GAMDM empirical model; 81-day running average).

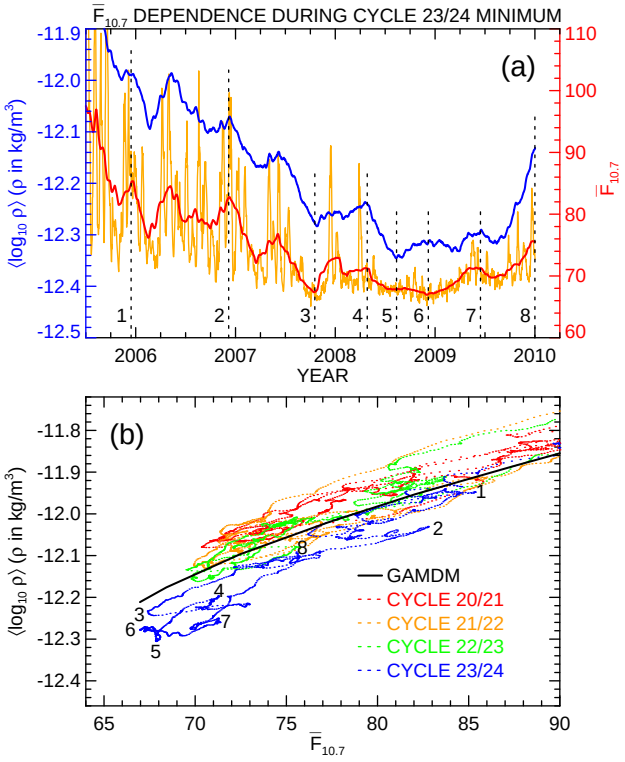

Figure 3. (a) 81-day average log-density at 400 km (blue), $\bar{F}_{10.7}$ (red), and daily $F_{10.7}$ (orange), as a function of time during the cycle 23/24 minimum. (b) Log-density versus $\bar{F}_{10.7}$ for the previous three solar minima (red, orange, green), for the cycle 23/24 minimum (blue), and from the GAMDM climatology (black). The numbered points correspond to the epochs marked by dotted lines in (a).

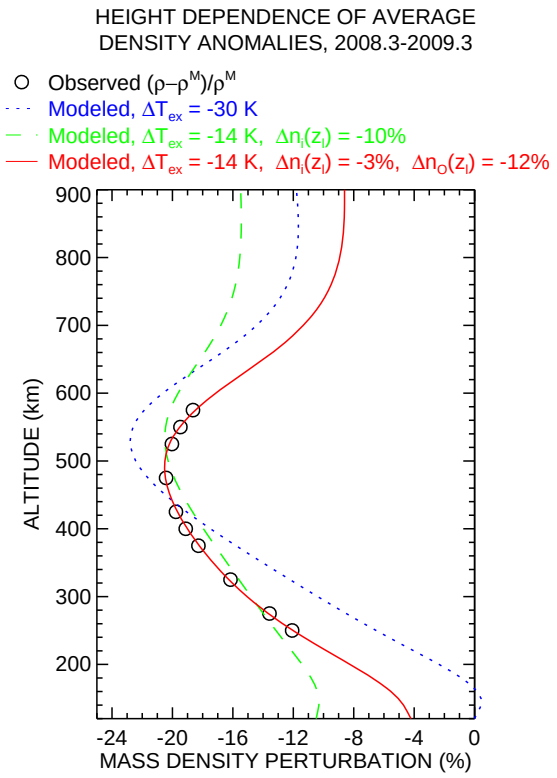

Figure 4. (Black circles) Height dependence of average density anomalies (relative to GAMDM) from 2008.3 to 2009.3. (Dotted blue line) Perturbation total mass density from a Bates-Walker (BW) diffusive equilibrium profile, in which exospheric temperature has been optimally perturbed to match the observed anomaly profile. The baseline BW parameters are from NRLMSISE-00. (Dashed green line) Same as dotted line, except that the number density of all species n_i at the base of the profile (z_l = 120 km) has also been perturbed. (Solid red line) Same as dashed line, except that the number density of O at z_l = 120 km has been perturbed independently of the other species.